Abschlussbericht zum Max-Buchner-Forschungsstipendium

In-situ Studies of Mass Transport in the FAME Epoxidation with Hydrogen Peroxide over Hierarchically Structured Molecular Sieve Catalysts

MBFSt-Kennziffer: 3427

Dr. rer. nat. Muslim Dvoyashkin
B. Sc. Marika Pelz

Institute of Chemical Technology
Universität Leipzig
Linnestraße 3-4
04103 Leipzig
Germany

muslim.dvoyashkin@uni-leipzig.de

1. Introduction and Objectives

In micro- and mesoporous materials, transport through pores occurs mainly by diffusion and often determines the overall rate of application processes such as adsorption or catalysis. While the vast majority of diffusion studies with advanced porous materials are performed with substances with small molecules, there is far less diffusion data in the literature for higher-molecular weight compounds with molecules up to several nanometers diameter, such as proteins, fats and oils or long-chain hydrocarbons. A specific example of the need for a much deeper understanding of transport of long-chain molecules in nanopores is the heterogeneously catalyzed epoxidation of fatty acid methyl esters (FAME) in the presence of microporous molecular sieves [1]. The catalytic oxidation of olefins to epoxides (oxiranes) is of great importance to the chemical industry. For instance, epoxides are valuable intermediates for a wide variety of bulk chemicals, polymers, and fine chemicals. Epoxidized fatty acid esters and their derivatives are attractive as renewable feedstocks [2]. In olefin epoxidation processes, the development of titanium-containing molecular sieves has received considerable attention in the last two decades. One such catalyst, titanium silicalite-1 (TS-1), has proven to be highly selective in the liquid-phase oxidation of a wide range of hydrocarbons, including alkenes, alkanes, alcohols, and aromatics. Epoxidation reactions with TS-1 can be performed at ambient temperatures and pressures using hydrogen peroxide as the oxidant, thus forming only water as a byproduct. The unique properties of TS-1 with hydrogen peroxide as the oxidant have been attributed in part to the hydrophobicity of the mostly siliceous structure. However, utilization of the microporous zeolites, such as e.g. titanium silicate (TS-1), is limited due to the size of its micropores, and, thus, strong limitations on diffusion inside the zeolite framework. Therefore, zeolites with hierarchical pore systems, in which a secondary pore system with larger pore size than the microporous facilitates intra-crystalline transport, are becoming attractive alternatives. In such materials, the presence of pores and channels of larger dimensions might help to overcome the transport limitations often associated with catalytic conversion over conventional zeolites.

In this context, the main focus of the present project is placed on the preparation of hierarchically structured catalyst by introduction of a secondary porosity (mesoporosity) into microporous TS-1 catalysts, and the subsequent direct assessment of the transport properties of the long-chain molecules, such as fatty acid methyl esters, confined to such a hierarchically structured pore system by means of gradient NMR techniques.

2. Material Preparation

Nano-sized titanium silicalite-1 with stacked morphology (**TS-1**) was prepared according to [3] by microwave-assisted synthesis. Typically, 36.5 g tetraethyl orthosilicate (TEOS, >99%, Merck), 35.7 g tetrapropylammonium hydroxide (TPAOH, 10 wt.% aqueous solution, Sigma Aldrich) and deionized water (39.2 g) were mixed under stirring for 1 h. 0.71 g titanium(IV) isopropoxide (TIP, 97%, Sigma Aldrich) and 8.15 g isopropanol (99%, BDH Prolabo) were mixed under stirring in a separate beaker for 45 min. Subsequently, the solutions were combined and stirred first for 2 h at room temperature and then at 353 K for 1 h to remove isopropanol. The resulting mixture was partitioned to 42 cm^3 each, added to a 100 cm^3 PTFE autoclave and transferred to a microwave oven (MLS, Start 1500) for crystallization. For that purpose, the synthesis mixture was heated for 5 min with an irradiation power of 600 W to 438 K and held at this temperature under autogeneous pressure for 70 min. After cooling to room temperature, the obtained solid was recovered by centrifugation, washed five times with 25 cm^3 deionized water, dried at 393 K for 6 h and calcined in an air atmosphere at 823 K for 6 h.

Hierarchically structured TS-1 was prepared by a two-step post-synthetic modification including partial desilication, followed by a hydrothermal pseudomorphic transformation (**TS-1_D**) with a subsequently recrystallization in presence of cetyltrimethylammonium cation $CTMA^+$ (OH^-/Br^-) (**TS-1_R**). Desilication was carried out by alkaline treatment of 3 g of the parent TS-1 with 50 cm^3 of NH_3 (25 wt.% aqueous solution, 13 M, AnalaR NORMAPUR, BDH Prolabo) NH_3 and tetrapropylammonium cation TPA^+ (TPAOH, 10 wt.% aqueous solution, 1.0 M Sigma Aldrich) as an additional structure-directing agent under reflux to 338 K. The resulting suspension was left to react for 70 min. After quenching to room temperature the solids were separated by

centrifugation, washed with deionized water until neutral reaction of the washing water, drying at 358 K and calcination in air at 813 K for 5 h.

For pseudomorphic transformation 1 g of the TS-1_D was mixed under stirring with an aqueous solution 21 cm^3 CTMAOH (0.08 M) and 21 cm^3 CTMABr (0.08 M). The CTMAOH solution was prepared by ion exchange of 1 g CTMABr (99%, Acros) dissolved in 42 cm^3 deionized water with 10 g Ampersep (900 OH, Fluka) at room temperature for 15 h. The resulting suspension was transferred to a polypropylene flask (Nalgene, V = 50 cm^3) and held at 383 K for 24 h. Then, the resulting solid was removed by filtration, washed five times with 25 cm^3 deionized water and once with 20 cm^3 anhydrous ethanol (99%, BDH Prolabo) and dried in air at 363 K for 15 h. The obtained materials were calcined in air at 473 K for 2 h, at 673 K for 2 h, and at 813 K for 15 h with a heating rate of 10 K min^{-1} between each of the steps.

3. Material Characterization

The powder XRD patterns of all TS-1 materials exhibit reflections coincident with the MFI framework topology (Fig.1). For the reflection at 2Θ = 25.40, which is characteristic for crystalline titanium dioxide (TiO_2) in the anatase modification, no significant intensity is observed. In comparison to the parent TS-1, a significant reduction in the intensity of the diffraction reflections is observed for the desilicated TS-1_D. The recrystallized TS-1_D_T shows a relative degree of crystallinity slightly higher than that of the parent TS-1. These results suggest that desilcation cause partial disrupt of the framework while recrystallization recovers the zeolitic phase due to the healing of defects. Scanning electron microscopy concludes that the parent TS-1 exhibits puck like crystals of sub micrometer sizes and a stacked morphology (Fig. 1, inset).
Nitrogen adsorption-desorption isotherms are shown in Fig. 2. The parent TS-1 zeolite exhibits a reversible type I isotherm (according to the IUPAC classification) with a steep rise at relative pressure $p/p_0 < 0.01$, confirming its microporous character, though having an enhanced uptake at higher relative pressures $p/p_0 > 0.9$. That uncommon uptake can be attributed to the stacked morphology hence the partial existence of larger mesopores. The parent TS-1 possess a BET surface area of 433 $m^2\ g^{-1}$ in which 13 $m^2\ g^{-1}$ is contributed by “external” surface area from t-plot analysis.

Desilication and transformation of TS-1 leads to isotherms representing combined type I and type II behavior. The isotherm of TS-1_D shows a remarkably enhanced uptake of nitrogen at higher relative pressures of p/p_0= 0.85 as well as a distinct H2 type hysteresis loop with a forced closure at aprox. 0.42 is observed.

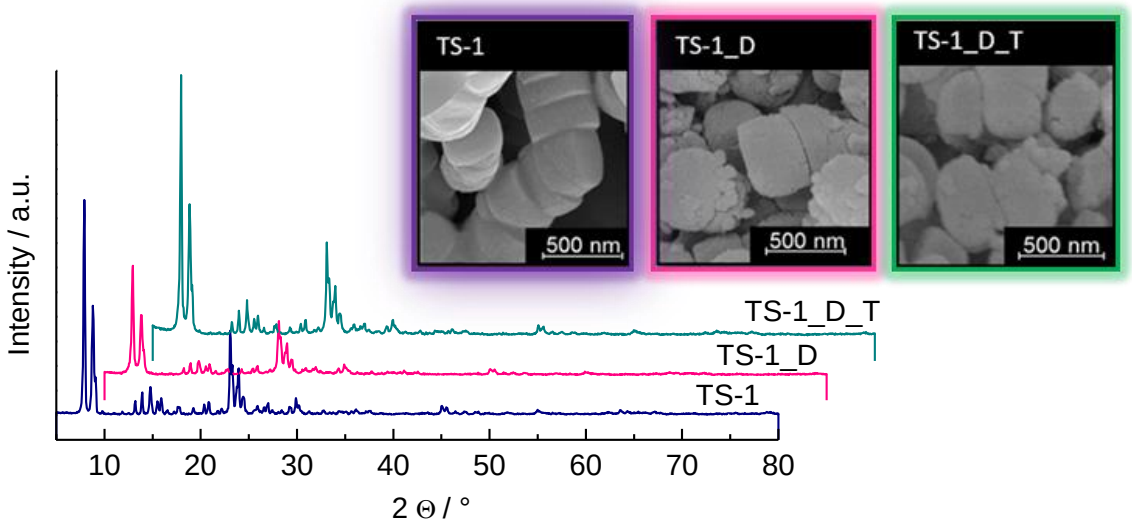

Fig. 1: Powder X-ray diffraction patterns of TS-1, desilicated TS-1_D and transformed TS-1_D_T. The inset in the top right corner contains the SEM images of the corresponding materials.

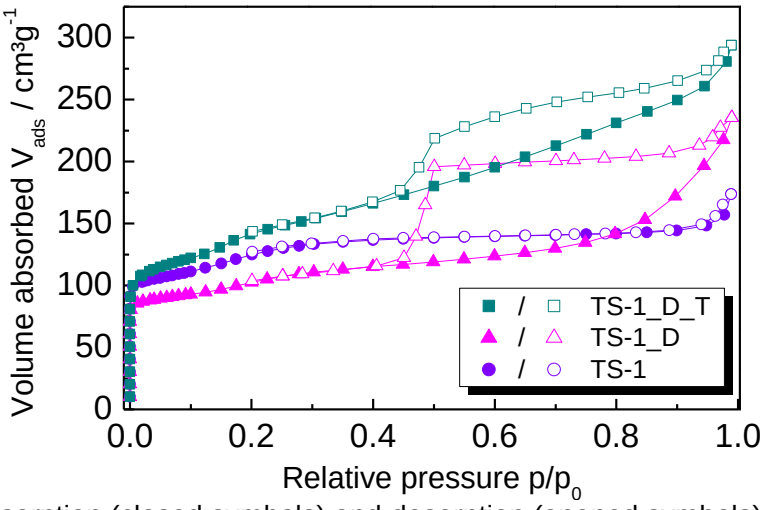

Fig. 2: Nitrogen adsorption (closed symbols) and desorption (opened symbols) isotherms of TS-1, desilicated TS-1_D and transformed TS-1_D_T catalysts.

The steep closing of the hysteresis loop is typical for mesoporous systems with pore openings considerably smaller than diameter of the inner pores, e.g. for ink-bottle shaped pores or partially constricted interconnected porous system. On the contrary to TS-1_D for the transformed material TS-1_D_T the uptake of nitrogen in the relative pressures range of p/p_0= 0.3-0.8 is more pronounced and indicate the presence of smaller mesopores (3-10 nm), which is in good agreement with the substantially enhanced contribution of the mesopore volume in the range of 3-10 nm (cf. Tab. 1). It is also notable that the hysteresis loops are less pronounced than in the desilicated materials and can be assigned to a combined H2 and H4. Compared to the non-treated TS-1 significantly increased mesoporosity is developed in the desilicated TS-1_D ($V_{10\text{-}40nm}$ = 0.11 cm^3g^{-1}) accompanied by a reduction of the micropore volume (cf. Tab. 1) and a decrease in the specific BET surface are (358 m^2 g^{-1}). The transformed TS-1_D_T exhibits a specific BET surface area of 483 m^2 g^{-1}, 130 m^2 g^{-1} higher than that of the TS-1_D material. In addition, 235 m^2 g^{-1} is contributed from the "external" surface.

Tab. 1: Titanium content and textural properties of TS-1, TS-1_D and TS-1_D_T catalysts.

	ω_{Ti} [a] / wt.%	V_{mikro} [b] / cm^3g^{-1}	$V_{3\text{-}10nm}$ [c] / cm^3g^{-1}	$V_{10\text{-}40nm}$ [c] / cm^3g^{-1}	A_{mikro} [b] / m^2g^{-1}	A_{ext} [b] / m^2g^{-1}	$A_{S,BET}$ [d] / m^2g^{-1}
TS-1	0.90	0.20	n.d.	n.d.	420	13	433
TS-1_D	1.00	0.13	0.04	0.11	280	78	358
TS-1_D_T	1.10	0.13	0.13	0.05	248	235	483

[a] from ICP-OES [b] t-plot- DeBoer [c] BJH [d] BET n.d. not determined

This results are believed to be directly related to the increased mesopore volume in the range of 3-10 nm ($V_{3\text{-}10nm,\ TS\text{-}1\_D\_T}$ = 0.13 cm^3g^{-1} vs. $_{TS\text{-}1\_D}$ 0.04 cm^3g^{-1}) (Tab. 1) and give the proof of a surfactant-assisted recrystallization during pseudomorphic transformation. The experimental procedure and the results of the epoxidation of FAME with H_2O_2 over the presented catalysts are described in the Ref. [4] It was believed that undefined (10-40 nm) and irregular shaped mesopores with possibly reduced accessibility incorporated by desilication have a negative impact on the catalyst efficiency (conversion related to the amount of Ti atoms in the catalysts). Thus, over the desilicated TS-1_D the catalyst efficiency and epoxide selectivity were reduced compared to the purely microporous TS-1 (TS-1_D 0.39 % μmol^{-1}; S_{eFAME} 77 % vs. TS-1 0.87 % μmol^{-1}, S_{eFAME} 81 %). More uniform mesopores in the range of 3-10 nm as present in the recrystallized TS-1_D_T are most beneficial for the catalytic efficiency. Thus, over the recrystallized TS-1_D_T a catalyst efficiency of 1.29% μmol^{-1}, which is 1.5 times higher with respect to the initial untreated TS-1, is observed and the epoxide selectivity reaches 79%.

In order to address potential accessibility issues for methyl oleate within mesopores of desilicated TS-1_D and desilicated and transformed (TS-1_D_T), diffusion studies allowing the direct determination of the self-diffusion coefficients of methyl oleate confined to mesopores were conducted.

4. PFG NMR Studies

The PFG NMR method has been employed as a well-suited, non-invasive tool in all sets of our diffusion measurements [5-7]. Diffusion studies were performed by ^{1}H pulsed field gradient (PFG) NMR using a wide-bore 9.4 T Bruker BioSpin spectrometer. It is equipped with a home-built gradient unit producing ultra-high *z*-gradients of up to 35 T/m in a 7mm o.d. NMR sample compartment .

NMR samples were prepared in a 7 mm o.d. glass tubes. Around 150 mg of each sample (TS-1, TS-1_D and TS-1_D_T) was placed within the NMR tube. Each NMR tube was then connected to a custom made vacuum system, and samples were activated under high vacuum (10^{-5} – 10^{-4} mbar) at around 400 K for overnight. After cooling them down to room temperature, each of the samples was saturated under vacuum by injection of methyl oleate (99%, Sigma Aldrich) and acetonitrile (99.8%) separately. The amount of liquids was chosen to be sufficient to cover the particles of the samples completely. This was done to ensure that all micropores (when acetonitrile is used) and mesopores (for acetonitrile and methyl oleate) were completely filled. After loading, the NMR tubes were detached from the vacuum system by flame sealing. This method of the sample saturation implies that in addition to the molecules in the micro- and mesopores, there will always be a fraction of molecules that is outside the porous particles, which will contribute to the observed NMR signals, too.

A stimulated echo (STE) pulse sequence [8] has been applied with the following parameters of the pulse sequence: τ = 2 ms, δ = 500 μs, and Δ = 8, 18, 40 and 160 ms. Here, τ is the spacing between the first two (π/2) pulses, δ is the effective duration of the gradient pulses, and Δ is the gradient pulses separation. The signal accumulation was performed with a repetition time of 5 times of T_1, where T_1 is the spin-lattice relaxation time of the component having the longest relaxation in the system. Additionally, selected diffusion experiments were carried out using the 13-interval pulse sequence [9] with the same values of diffusion times and gradient amplitudes used in experiments with STE. This was done in order estimate a possible effect of the internal magnetic fields originating from the susceptibility differences between the fluid and the porous material and effects of undesirable eddy current effects. A small difference within the range of experimental uncertainty was observed (Fig. 3). These experiments were conducted for two different diffusion times – 8 ms and 18 ms.

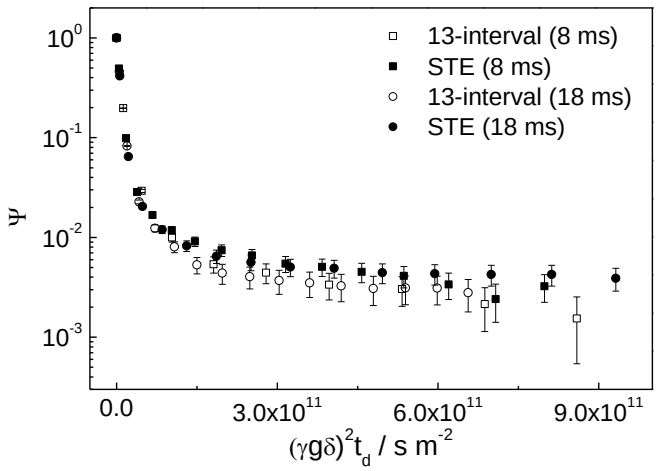

Fig. 3: ^{1}H PFG NMR diffusion attenuation curves measured for methyl oleate adsorbed in TS-1_D_T at 298 K. The data obtained by 13-interval and STE pulse sequences are represented by open and solid symbols, respectively. Presence of an additional pair of gradient pulses in the 13-interval pulse sequence has been taken into account plotting values of $(\gamma g \delta)^2 t_d$.

Generally, the decrease of the measured NMR signal (ψ) caused by diffusion for a system containing molecular ensembles (p_i) with different diffusion coefficients (D_i), and being in the slow (compared to the time of the experiment) diffusion exchange can be presented in the form [5]:

$$\psi(g\delta, t_d) = \sum_i p_i \cdot exp(-D_i\gamma^2 g^2 \delta^2 t_d) \qquad (1)$$

where γ - is the gyromagnetic ratio of the nucleus that is observed, g and δ are the amplitude and the duration of the gradient pulses, respectively, t_d is the effective diffusion time ($[\Delta - \delta/3]$ in case of STE and $[\Delta - \delta/6 - \tau/2]$ of the 13-interval pulse sequence). Under conditions of a fast diffusion exchange, Eq. (1) transforms into:

$$\psi_{fast}(g\delta, t_d) = exp(-D\gamma^2 g^2 \delta^2 t_d) \qquad (2)$$

in which D – is the time-averaged diffusion coefficient of the exchanging ensembles $D = \sum_i p_i D_i$. For $i > 1$, Eq. (1) gives a poly-exponential decay of the observed NMR signal, while Eq. (2) results in a mono-exponential decay.

In the situation, when during the time of experiment t_d one ensemble of molecules (or a set of ensembles) is in the slow exchange with another set, which in turn is undergoing intermediate or fast exchange within its ensembles (the so-called long-range diffusion), a combination of Eqs. 1 and 2 can be used for the description of the diffusion attenuation curves.

Fig. 4 displays a number of diffusion attenuation decays measured for TS-1 (Fig. 4. A), TS-1_D (Fig. 4. B) and TS-1_D_T (Fig. 4. C) for diffusion times of 4, 18, 40 and 160 ms. As expected, and being consistent with the sample preparation procedure for NMR experiments, all attenuation curves are not mono-exponential. The existence of a significant fraction of the methyl oleate outside the pores, i.e., surrounding the crystallites of the catalyst, results in a component having the fastest diffusion decay close the value diffusivity of the bulk methyl oleate. The latter has been measured in the separate diffusion experiment with just bulk methyl oleate inside the NMR tube at the same temperature (298 K) and has resulted in the self-diffusion coefficient $D_{bulk}^{MO} = 1.7 \cdot 10^{-10}\, m^2 s^{-1}$. The decay that would correspond to this diffusivity is presented by a dashed line. The data presented on Fig. 4 can satisfactorily be fitted by Eq. 1 assuming the presence of at least 2 for the sample TS-1 and 3 for the samples TS-1_D and TS-1_T components having different diffusivities. Results of the fitting are summarized in the Tab. 2.

Thus, the presence of at least three components in the observed attenuation curves for the desilicated TS-1_D and the recrystallized material TS-1_D_T may be attributed to bulk-like diffusion of methyl oleate outside the porous crystallites, restricted diffusion within the mesopores, and the long-range diffusion. The latter is related to molecules which spend part of the time inside the mesopores and part of the time outside, i.e., which undergo an exchange between the intrparticle pore space and the space outside pores.

The slowest diffusivity D_3 observed for the parent TS-1 material ($5.0 \cdot 10^{-11}\, m^2 s^{-1}$, see Tab. 2) is more than one order of magnitude higher than the values obtained for desilicated TS-1_D ($2 - 4 \cdot 10^{-12}\, m^2 s^{-1}$) and transformed TS-1_D_T ($1.1 - 1.3 \cdot 10^{-12}\, m^2 s^{-1}$) materials. This suggests that for the TS-1 a component, which might diffuse within the micropores, is not observed. This is consistent with the results of the N_2-sorption isotherms of the TS-1 material (see Fig. 2) revealing that only micropores (~0.5 nm) are present. These are evidently and expectedly too narrow for the adsorption of the long-chain methyl oleate molecules. It is worth noting that the results for the fraction of molecules diffusion within mesopores p_3 might be affected by the longitudinal relaxation effects. To address this, accurate relaxation studies are planned in the future.

The root mean squared displacements (RMSDs) of the molecules possessing the slowest diffusivity can be estimated using the Einstein relation: RMSD=$\sqrt{6Dt_d}$. For the smallest observation time used in the experiment (8 ms) these were found to be ~1.2 μm and ~700 nm for the TS-1_D and TS-1_D_T, respectively. This is of the same order of magnitude as the sizes of individual crystallites seen in the SEM images (see Fig. 1). This suggests that the observed diffusivities D_3 are predominantly determined by the diffusion within mesopores.

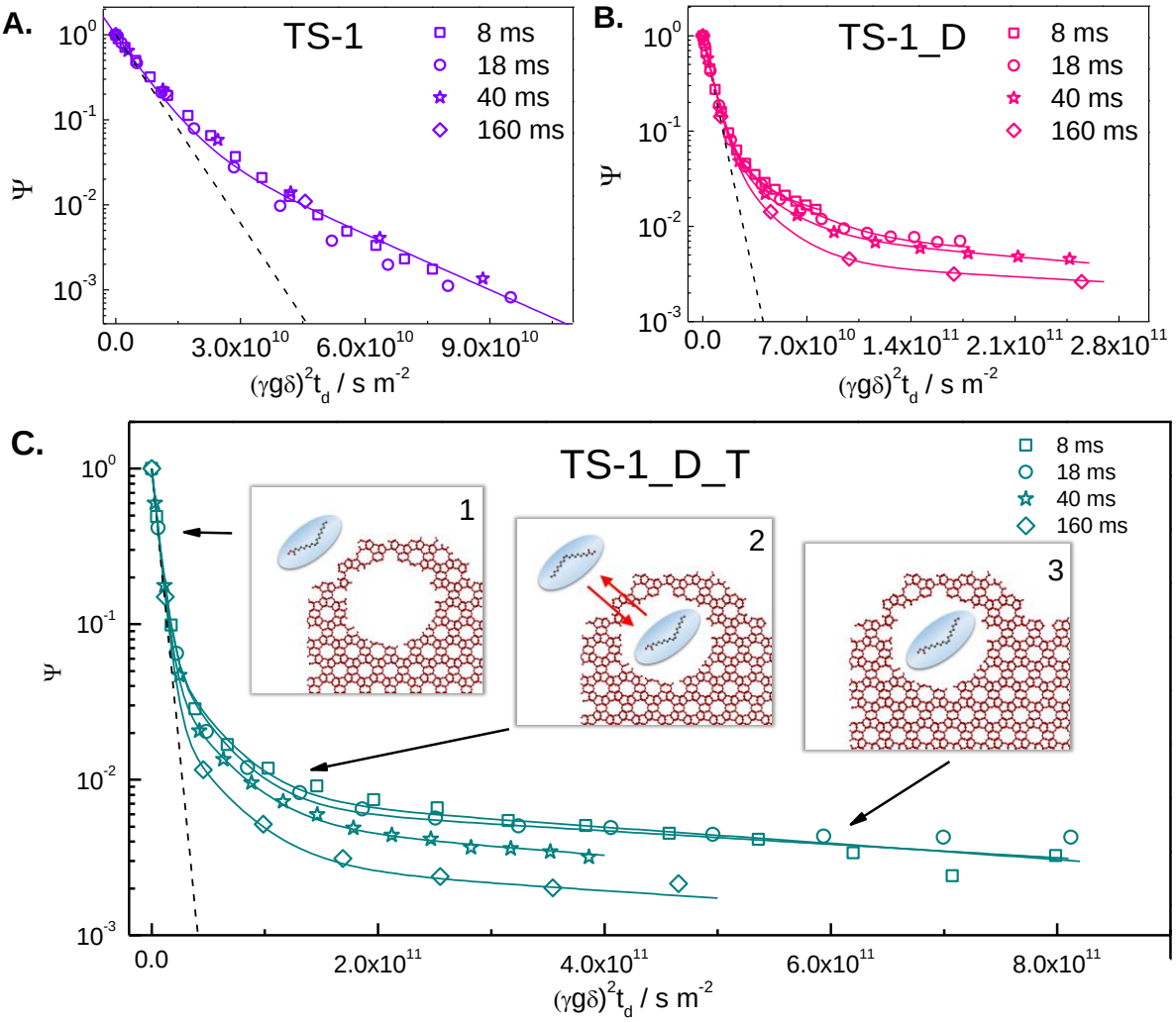

Fig. 4: ^{1}H PFG NMR diffusion attenuation curves obtained for methyl oleate adsorbed into TS-1 (A), TS-1_D (B) and TS-1_D_T (C) for 8 ms (squares), 18 ms (circles), 40 ms (stars) and 160 ms (diamonds) of diffusion time at 298 K. The solid lines represent the 2-exponential (A) and 3-exponential (B, C) fits of the data using Eq. 1. Dashed line represents the attenuation of the pure methyl oleate measured in a separate experiment. The schematics demonstrate what type of diffusion process is dominating in different sections of the attenuation curves: 1 – bulk-like diffusion outside pores, 2 – long-range diffusion caused by exchange between the spaces inside and outside pores, and 3 – diffusion within mesopores.

Tab. 2: Parameters resulting from the fitting of attenuation curves of Fig. 4 using Eq.1

	t_d / ms	p_1	D_1^* / x10^{-11} m^{2}s^{-1}	p_2	D_2 / x10^{-11} m^{2}s^{-1}	p_3**	D_3 / x10^{-12} m^{2}s^{-1}
TS-1	8-160	0.91	1.7	0.09	5±1	n/d	n/d
TS-1_D	8	0.92	1.7	0.06	4±1	0.017	3±1
	18	0.92	1.7	0.07	3±1	0.007	2±1
	40	0.92	1.7	0.07	4±1	0.009	3±2
	160	0.92	1.7	0.07	4.5±2.5	0.005	3±2
TS-1_D_T	8	0.92	1.7	0.07	2.8±0.3	0.009	1.2±0.2
	18	0.92	1.7	0.07	2.9±0.3	0.007	1.2±0.2
	40	0.95	1.7	0.05	2.6±0.8	0.005	1.3±0.7
	160	0.97	1.7	0.03	3±1	0.003	1.1±0.9

*Parameter $D_1 = 1.7\text{x}10^{-10}$ m^{2}s^{-1} was fixed in the fitting procedure.
** Uncertainty in determination of p_3 is close to 20%.

It also means that the methyl oleate molecules diffuse with a comparable rate within both catalysts. This should lead to the similar accessibilities for the methyl oleate to the active sites inside nanopores. However, activity of the transformed material (TS-1_D_T) was found to be notably higher [4]. The observe differences in activities, thus, have to from another effects, e.g., different surface hydrophlicity of the desilicated and transformed materials.

5. Conclusions and Perspectives

The introduction of secondary porosity in zeolitic crystals TS-1 by desilication and subsequent recrystallization results in the higher catalytic activity compared to the parent purely microporous material. In turn, PFG NMR studies demonstrate that the thus created mesoporosity does facilitate transport of bulky methyl oleate molecules into the zeolite particle, which is prohibited for the purely microporous TS-1 material.

The presented diffusion data also demonstrate feasibility of application of PFG NMR technique for the direct determination of diffusion coefficients of long-chain molecules (such as e.g. methyl oleate) in a various catalysts with hierarchically structured pore systems. Thus, the improved activity of desilicated and recrystallized TS-1 in the epoxidation of methyl oleate and biodiesel can be studied in more detail in the near future. In turn, this may provide insight into the role of mass transfer processes with respect to surface properties and/or intrinsic activity of the Ti sites in the catalysts.

6. Publications and Conference Contribution

The results of this work is partly published in the Ref. [4]. One more publication containing the reported diffusion data is planned for preparation. The results of this work are planned to be presented at 28. Deutsche Zeolith-Tagung (März 2016, Gießen) and at 49. Jahrestreffen Deutscher Katalytiker (März 2016, Weimar).

7. References

[1] N. Wilde, C. Worch, W. Suprun, R. Glaser, Microporous and Mesoporous Materials 164 (2012) 182-189.

[2] U. Biermann, U. Bornscheuer, M.A.R. Meier, J.O. Metzger, H.J. Schafer, Angewandte Chemie-International Edition 50 (2011) 3854-3871.

[3] H.L. Jin, N.Z. Jiang, S.M. Oh, S.E. Park, Top. Catal. 52 (2009) 169-177.

[4] N. Wilde, M. Pelz, S.G. Gebhardt, R. Glaser, Green Chemistry 17 (2015) 3378-3389.

[5] J. Kärger, H. Pfeifer, W. Heink, Advances in Magnetic Resonance 12 (1988) 2-89.

[6] A.R. Dutta, P. Sekar, M. Dvoyashkin, C.R. Bowers, K.J. Ziegler, S. Vasenkov, Chemical Communications 51 (2015) 13346-13349.

[7] M. Dvoyashkin, H. Bhase, N. Mirnazari, S. Vasenkov, C.R. Bowers, Analytical Chemistry 86 (2014) 2200-2204.

[8] R.M. Cotts, M.J.R. Hoch, T. Sun, J.T. Markert, Journal of Magnetic Resonance 83 (1989) 252-266.

[9] P. Galvosas, F. Stallmach, G. Seiffert, J. Karger, U. Kaess, G. Majer, Journal of Magnetic Resonance 151 (2001) 260-268.